PAPER

Physical–chemical properties of nanocomposites based on poly(3-hydroxybutyrate-co-3-hydroxyvalerate) and titanium dioxide nanoparticles

Materials Research Express

RECEIVED
28 September 2017

REVISED
22 November 2017

ACCEPTED FOR PUBLICATION
6 December 2017

PUBLISHED
4 January 2018

PAPER

Physical–chemical properties of nanocomposites based on poly(3-hydroxybutyrate-co-3-hydroxyvalerate) and titanium dioxide nanoparticles

Natália F Braga[1,3], **Ana Paula da Silva**[1], **Tatiane Moraes Arantes**[2], **Ana Paula Lemes**[1] and **Fernando Henrique Cristovan**[1]

[1] Department of Science and Technology, Federal University of São Paulo (Unifesp)—São José dos Campos 12231-280, SP, Brazil
[2] Department of Chemistry, Federal University of Goias (UFG)—Jatai 75801-615, GO, Brazil
[3] Author to whom any correspondence should be addressed.

E-mail: natyfbraga@hotmail.com, anapaula.silva.sjc@hotmail.com, tmarantes@ufg.br, aplemes@unifesp.br and fhcristovan@unifesp.br

Keywords: PHBV, titanium dioxide, nanoparticles, nanocomposites, physical–chemical properties, biodegradation

Abstract

Poly(3-hydroxybutyrate-co-3-hydroxyvalerate) (PHBV) was reinforced with titanium dioxide (TiO_2) in concentrations of 1.0%, 2.5% and 5.0% (m/m) to produce nanocomposites by the solvent casting technique. TiO_2 was synthesized by a hydrothermal treatment to produce nanoparticles. The nanostructure of the nanoparticles was studied by x-ray diffraction analysis (XRD) and transmission electron microscopy (TEM). The XRD confirmed TiO_2 crystalline nanoparticles, with a mixture of anatase and rutile phases. Through TEM analysis, the formation of TiO_2 nanorod agglomerates with an average diameter and length of 40 and 12 nm, respectively, was observed. The thermal and mechanical properties of the pure PHBV and nanocomposite films were characterized by differential scanning calorimetry (DSC) and dynamic mechanical analysis. The DSC analysis showed that the glass transition temperature decreased with the inclusion of TiO_2 in the PHBV matrix in relation to pure PHBV. The results of biodegradation assays for the PHBV and nanocomposites in an aqueous medium and in soil showed morphological and structural changes for all samples, indicating a high biodegradation rate for this material. The most important conclusion is that the biodegradation of the PHBV was not affected by the addition of nanoparticles, thus enabling the use of nanocomposites in applications requiring biodegradable materials.

1. Introduction

Due to current environmental issues, there is a necessity for the creation of viable alternatives in order to reduce the negative impacts on the environment. Therefore, the use of biodegradable polymers has increased in the last decade. Biodegradable polymers have a broad range of applications. For example, poly(lactic acid) (PLA) can be used for food packaging [1], while poly(glycolic acid) (PGA), poly(e-caprolactone) (PCL), polyhydroxybutyrate (PHB) and its copolymer poly (hydroxybutyrate-co-hydroxyvalerate) (PHBV) can be used to fabricate scaffolds in tissue engineering [2]. Furthermore, PHBV is a natural microbial polyester with good properties and is also biocompatible and biodegradable [3].

The application of a material often requires new properties that a pure polymer may not have. One of the ways to modify the properties of the polymer to satisfy such needs is by the incorporation of nanoparticles. In this case, the material is called a polymer nanocomposite.

The dispersion of nanoscale particles within a polymer matrix results in nanocomposites with considerable improvements regarding their physicochemical properties [4]. Nanoparticles can be introduced in the polymer matrix in order to enhance the mechanical and functional properties of the nanocomposites compared to conventional microcomposites [5, 6]. Generally, polymer nanocomposites are the result of a combination of

polymers and inorganic/organic fillers at the nanometer scale [5]. Reinforcing fibers of various sizes and forms have been effectively used in polymer composites as reinforcing agents. Nanofillers, however, are found to be preferential in several applications, due to their high surface area and the lower concentrations needed to achieve the reinforcement effect [7].

Considering the factors discussed above, it can also be noted that titanium dioxide (TiO_2) has been used in many industrial processes due to its exceptionally efficient photoactivity, high chemical stability and low cost [8]. There are several works related to polymer properties, such as degradation behavior [9, 10], thermal stability [9, 11–13], dynamic mechanical properties [11, 14] and morphology [9], with the presence of small amounts of TiO_2. TiO_2 is a good candidate for biological applications, including the manufacturing of bone implants due to its surface morphology. Because of its nanotopography, it plays an important role in mechanical interlocking with surrounding bones, favorably influencing the adhesion, proliferation and differentiation of osteoblasts [15, 16]. The insertion of TiO_2 nanoparticles promotes an increase in the hydrophilicity of the matrix surface. Substrates that are more hydrophilic increase the interaction of the polymer matrix with the cells and consequently improve their integration into the tissue [17–19]. Thus, cell adhesion is of extreme importance for the science of biomaterials. In addition, the TiO_2 layer formed naturally on the surface of titanium implants is biocompatible and favors osseointegration, as this layer provides the surface nucleation of hydroxyapatite and thus favors bone integration. This favoring is due to the surface hydroxyl groups of titanium oxide (Ti–OH), which present a negative surface charge for attracting calcium ions, thus initiating the nucleation of hydroxyapatite [20, 21]. The use of TiO_2 nanoparticles can be a new route to enhance some properties of PHVB, such as biodegradability.

This study considers the introduction of nanostructures in biodegradable polymer matrices to obtain nanocomposites with specific properties. Specifically, this work provides a baseline study focused on the preparation and characterization of nanocomposites based on the polymer PHBV with the insertion of titanium dioxide nanoparticles.

2. Experimental section

2.1. Materials

PHBV was supplied by PHB Industrial S/A (used as received). PHBV has a molecular weight of 230 000 g mol^{-1} with 15% hydroxyvalerate units. Titanium isopropoxide (IV), $Ti\{OCH(CH_3)_2\}_4$ and hydrogen peroxide (H_2O_2, 30% in volume) were purchased from Sigma Aldrich. Finally, deionized water with $R = 18$ mΩ cm^{-1} was used.

2.2. Synthesis of TiO_2 nanoparticles

In this work, TiO_2 nanoparticles were produced by the method described by Ribeiro *et al* [22], but with modifications. This process is based on the hydrothermal treatment of the peroxo complex of a titanium (PCT) gel solution. The PCT gel was prepared from titanium isopropoxide (IV), $(Ti(OCH(CH_3)_2)_4$ and hydrogen peroxide (H_2O_2, 30% in volume). In a typical synthesis process, 2.84 g of titanium isopropoxide was slowly added to 11.3 g of hydrogen peroxide, 10:1 mol% H_2O_2/Ti, under vigorous stirring in an ice bath to prevent the hydrogen peroxide decomposition. The final solution volume was then adjusted to 100 ml in a flask with deionized water. The flask was connected to a reflux apparatus to prevent water evaporation and was kept refluxing at 80 °C in an oil bath. A yellow gel was obtained after 15 min.

An aliquot of 10 g of the gel was dissolved in 90 ml of deionized water in a flask containing an autoclavable screw cap and then placed in an oven and subjected to a constant temperature (120 °C) for 48 h, thus precipitating the TiO_2 nanoparticles by the thermal destabilization of the PCT gel. The colloidal dispersion containing the nanoparticles was dried in an oven at 90 °C in order to remove the nanoparticles.

2.3. Preparation of nanocomposites

The PHBV and nanocomposite films were prepared by the solvent casting technique. The polymer was dissolved with chloroform (15% m/v), through stirring and heating for 30 min, until dissolution was completed. After this step, suitable amounts of titanium dioxide were added to each solution and stirred to promote homogeneity. The nanocomposites were prepared with 1.0%, 2.5% and 5.0% m/m of nanoparticles/PHBV. Then, the solution was transferred to a petri dish and, after solvent evaporation, the films were obtained.

2.4. Characterization

The titanium dioxide nanoparticles were characterized by x-ray diffraction (XRD) using a Rigaku model DMax 2500PC diffractometer, operated with Cu Kα radiation with $\lambda = 1.5406$ Å. The scanning range was from 10° to 110°, with an angle step of 0.01° and a time step of 1 s. The crystallographic domain (crystallite size) of the TiO_2 nanopowders was determined considering the most intense peaks, (101) for anatase and (110) for rutile planes in

the TiO_2 pattern, using the Scherrer equation [23]. The nanoparticles were also analyzed by transmission electron microscopy (TEM) with a Philips model CM 120 microscope, with thermoionic filament LaB_6 and an acceleration voltage of 120 KV. The samples were placed on a copper grid that was covered with a thin layer of carbon.

The PHBV and nanocomposite films were analyzed by Fourier transform infrared (FTIR) spectroscopy in an absorption spectrometer in the infrared region using a Shimadzu model—IRAffinity-1 with an attenuated total reflectance accessory (ZnSe). The operating conditions were the region of 500–4000 cm^{-1}, 16 scans and a resolution of 2 cm^{-1}.

The measurements of differential scanning calorimetry (DSC) for the PHBV and nanocomposite films were performed by a thermogravimetric analyzer with a thermal differential scanner NETZSCH model DSC 204 Phoenix, with an empty aluminum crucible in a nitrogen atmosphere as a reference. The samples were cooled to −20 °C in nitrogen atmosphere and then heated to 200 °C at a rate of 10 °C min^{-1}, maintained at this temperature and, after that, cooled to 0 °C at a rate of 10 °C min^{-1}. The second heating was up to 200 °C at the same heating rate.

The viscoelastic properties of PHBV and the nanocomposites were determined by dynamic mechanical analysis (DMA) using DMA 2980, TA instruments Q800, with a frequency of 1 Hz in strain mode. The measurements were performed with samples in the form of rectangular films (30 mm × 5 mm). The scans occurred in the temperature range from −80 °C to 50 °C with a heating rate of 2 °C min^{-1} and an amplitude of 20 μm.

2.5. Biodegradation tests

In this work, the biodegradation was studied both in an aqueous medium and in soil. The biodegradation in the aqueous medium was carried out in a vessel containing a nutrient solution in a similar method descripted by Hong *et al* [24] and Silva *et al* [25]. Films of PHVB and its nanocomposites, containing 1.0%, 2.5% and 5.0% of TiO_2, were immersed in this medium for 10 d. For the biodegradation test in soil, the films were buried in garden soil with a depth of 40 mm. The humidity was controlled at 60% of the retention capacity for 20 d in an oven at 28 °C (Silva *et al* [26]).

In both tests, the pure PHBV films were also placed under the same conditions for comparison purposes. The triplicate films were retrieved from the aqueous medium or the soil, washed in distilled water, dried in the desiccator and weighed. The degradation of these films was evaluated in terms of weight loss percentage.

3. Results and discussion

3.1. Synthesis of titanium dioxide nanoparticles

Several methods can be employed to produce titanium dioxide nanopowders, such as chemical vapor deposition [27], oxidation of titanium tetrachloride [28] and flame synthesis [29]. Nowadays, the most used method to industrially produce TiO_2 is based on a plasma spray synthesis technique, which allows high productivity but leads to the production of impure nanoparticles. The production of nanoparticles by chemical precipitation is the best method to assure a high degree of purity for the final product [30]. Several studies regarding the synthesis of titanium dioxide can be found in the literature [31–33]. Anwar *et al* [34] synthesized titanium dioxide nanoparticles via a low-temperature sucrose ester micelle-mediated hydrothermal processing route using titanium isopropoxide as the precursor. They observed mixed crystalline phases, consisting of anatase (main phase) and brookite. They also reported a change in morphology under certain conditions. Upon increasing the hydrothermal reaction temperature, the morphology of the nanoparticles transformed from spheres to rods. In the present work, TiO_2 nanoparticles were produced using the method reported by Ribeiro [22]. Through this method, stable colloidal nanoparticles can be obtained with good shape and size control. It is possible to produce nanorods with lengths and diameters of ~40 and 12 nm, respectively, which provide effective dispersion in the polymer matrix, resulting in homogeneous nanocomposites.

The TiO_2 nanoparticles obtained in this work were structurally characterized by XRD. The TiO_2 nanoparticle XRD patterns are presented in figure 1(a). The peaks observed were attributed to a mixture of anatase and rutile phases, in accordance with Joint Committee on Power Diffraction Standards (JCPDS) cards 21-1272 and 21-1276, respectively. The quantity of each crystalline phase present in the sample was calculated based on the (101) peak area for the anatase phase (JCPDS # 21-1272) and (110) peak area for the rutile phase (JCPDS # 21-1276), according to:

$$Xa = \left(\frac{Aa}{Aa + Ar}\right) * 100, \quad (1)$$

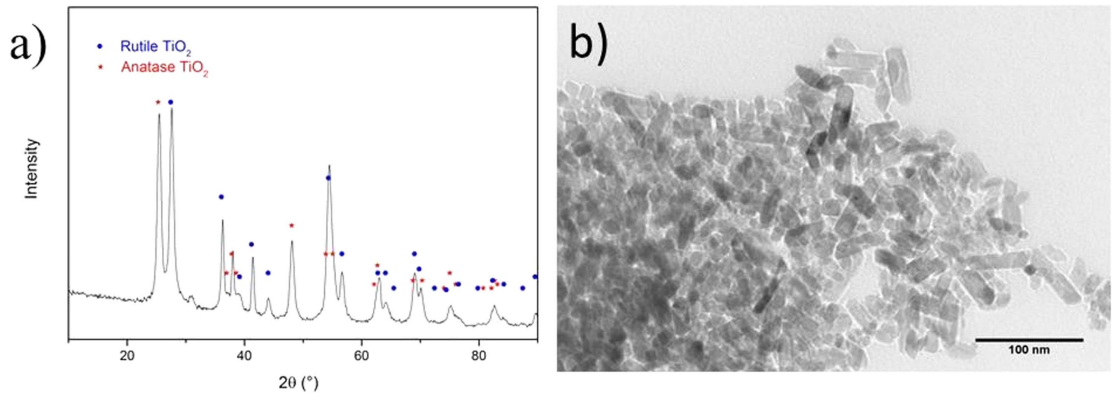

Figure 1. (a) XRD pattern of TiO_2 nanoparticles. (b) TEM image of TiO_2 nanoparticles.

Table 1. Crystallographic coherence domain for planes of the anatase and rutile phases.

Anatase phase		Rutile phase	
Plane	Crystallographic coherence domain (nm)	Plane	Crystallographic coherence domain (nm)
101	10.1	101	16.2
200	10.0	211	8.2
204	8.7	111	16.8
220	9.9	210	9.5

where Xa is the quantity of anatase phase, Aa is the (101) peak area for the anatase phase and Ar is the (110) peak area for the rutile phase. Using this equation, it was possible to estimate that the percentages of rutile and anatase phases were the same (50% of each phase).

The crystallographic coherence domain (crystallite size) for the nanoparticles was estimated using the Scherrer equation [23]:

$$\mathrm{CD} = \frac{k\,\lambda}{\beta\,\cos\Theta}, \tag{2}$$

where CD is the crystallographic coherence domain, k is a constant, λ is the wavelength associated with the x-ray radiation, β is the full width at half maximum for the band in the diffraction peak and Θ is the diffraction angle.

The crystallographic coherence domain values estimated by the Scherrer equation for some planes of the anatase and rutile phases from the diffractogram in figure 1(a) are shown in table 1.

As shown in table 1, an average crystallite size was obtained for the anatase phase (~10 nm), but the values calculated for different crystallographic orientations were also close to 10 nm, indicating that there was no preferential growth in a specific direction. This indicates that the nanoparticles in this phase have spherical symmetry. For the rutile phase, the crystallographic coherence domain varied greatly depending on the direction of the crystallographic plane. As a result of this, it was possible to observe rod formations in the micrographs obtained by TEM for the nanoparticles.

The morphology of the nanoparticles was characterized by TEM. The micrographs are shown in figure 1(b). The formation of nanorod agglomerates are observed, with diameters and lengths of the order of 12 and 40 nm, respectively. These nanoparticles can be associated with the rutile phase, considering the calculated crystallographic coherence domain and the rod format. Crystallite sizes can sometimes be smaller than those observed by electronic microscopy, indicating that particles were formed by the union of smaller blocks [35].

3.2. PHBV and PHBV/TiO_2 nanocomposite films

In this study, nanocomposites of PHBV and titanium dioxide were prepared at room temperature using the solvent casting technique, resulting in films containing 1.0%, 2.5% and 5.0% TiO_2, with a thickness of ~0.5 mm.

The FTIR technique was used to study the interactions between the nanoparticles and the polymer matrix. The FTIR spectroscopy results for PHBV and the nanocomposites are shown in figure 2. In the PHBV spectrum, there are bands associated with stretching vibrations of the C–O–C group in the range of 1245–1319 cm^{-1}. In

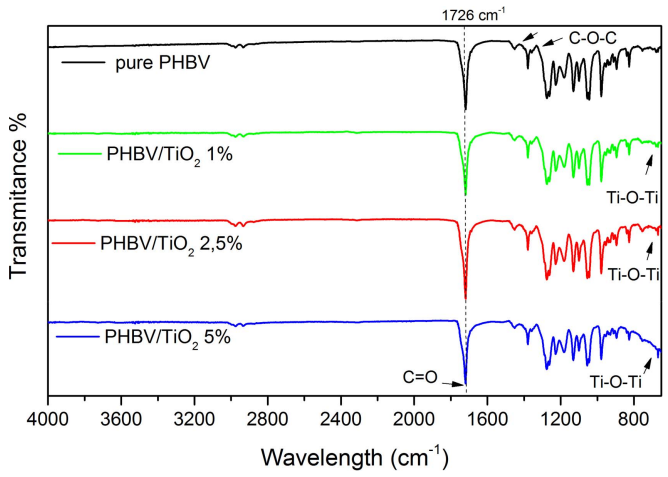

Figure 2. FTIR spectra of PHBV and nanocomposites.

Table 2. Thermal properties of PHBV and the nanocomposites.

	First heating		Cooling		Second heating					
	T_m (°C)	ΔH_m (J g^{-1})	T_c (°C)	ΔH_c (J g^{-1})	T_g (°C)	T_{cc} (°C)	T_m (°C)	ΔH_m (J g^{-1})	ΔH_{cc} (J g^{-1})	%C*
Pure PHBV	172.3	50.2	54.1	2.3	−1.8	56.4	170.2	48.4	36.0	8.5
1.0% TiO_2	172.9	48.7	47.1	1.4	−3.4	55.1	170.0	46.6	36.1	7.3
2.5% TiO_2	172.8	47.1	54.7	2.6	−1.9	56.5	170.4	43.8	32.5	8.0
5.0% TiO_2	170.3	53.5	52.1	29.9	−7.0	46.8	169.0	52.8	16.7	26.0

addition, there are bands associated with the stretching of the C=O double bond in the range of 1700–1760 cm^{-1} [36]. The bands in the regions of 2960–3015, 2925–2945 and 2865–2885 cm^{-1} are associated with the asymmetric stretching modes of CH_3, anti-symmetric stretching modes of CH_2 and symmetrical stretching modes of CH_3, respectively. The bands in the region of 800–1500 cm^{-1} are associated with the bending vibrations for CH_3 and CH [37]. Figure 2 also shows that the nanocomposite spectra are very similar to the one for pure PHBV, but with an absorption peak in the region of 500–800 cm^{-1} associated with Ti–O–Ti stretching observed [38]. These signals are in accordance with those described by Peng *et al* [39], who studied PET/TiO_2 nanocomposites.

The thermal properties related to the crystallization and melting processes were analyzed by DSC for the films. Table 2 shows the values obtained from the thermograms, such as the melting temperature (T_m), melting enthalpy (ΔH_m), crystallization temperature (T_c), crystallization enthalpy (ΔH_c), glass transition temperature (T_g), cold crystallization temperature (T_{cc}), cold crystallization enthalpy (ΔH_{cc}) and degree of crystallinity (%*C*), which was calculated from:

$$\%C = \frac{\Delta H_m - \Delta H_c}{\Delta H_{m100\%} \times W} \times 100, \quad (3)$$

where the theoretical $\Delta H_{m100\%}$ of a hypothetical 100% crystalline polymer is known. The value used for ΔH_m100% was 146 J g^{-1} [40] for PHBV and W is the mass fraction of PHBV in the mixture.

Figure 3 shows the DSC results for PHBV and the nanocomposites. It was found that the pure PHBV samples showed two endothermic peaks, the first at 157.8 °C and the second at 172.5 °C, as can be observed in the first heating curve (figure 3(a)). Double or multiple melting peaks may happen due to partial melting, recrystallization and reflow during heating, polymorphism, the existence of different crystalline morphologies (thickness, distribution, completeness or lamellar stability), physical aging and/or relaxation of a rigid amorphous phase, or species with different molar masses [41]. According to Casarin [42], for PHBV with percentages of valerate above 5%, a nonhomogeneous distribution in the polymer chains takes place, which causes a change in the molecular mass. This change can also be observed in this study, because the PHBV used in this work had 15% valerate. In addition, Buzarovska *et al* [43] stated that the first peak is probably associated with the homogeneous nucleation of PHBV, which begins spontaneously by aggregation of the chains below the melting point, and the second peak is probably associated with the heterogeneous nucleation of PHBV. Other

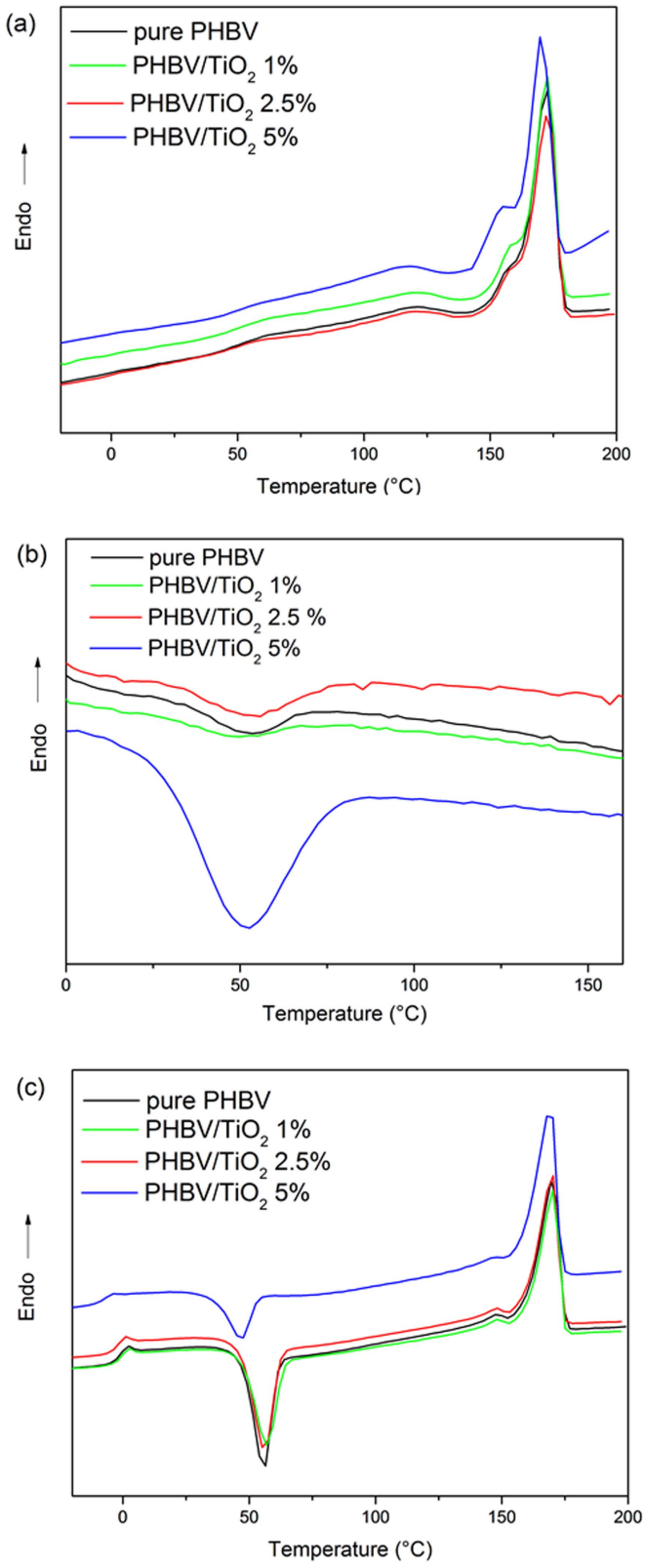

Figure 3. DSC curves of the pure PHBV and nanocomposites: (a) first heating, (b) cooling and (c) second heating.

authors have also reported two endothermic peaks in PHBV and its nanocomposites [42, 43]. Vidhate *et al* [45] studied DSC analyses of PHBV/MWNTs and showed that, for pure PHBV, the upper melting peak was dominated with the increase of heating rates. However, for the nanocomposite, the lower melting peak was more pronounced. In DSC measurements of PHBV/LDH nanocomposites, Dagnon *et al* [44] suggested that the bimodal endothermic melting peak for the first heating appears due to the presence of two crystalline phases in the sample.

Figure 3(b) shows the cooling thermogram, where the endothermic peak is not observed for any sample. The crystallization temperature (T_c) can be observed at 54.1 °C, 47.1 °C, 54.7 °C and 52.1 °C for PHBV and for the nanocomposites with 1.0%, 2.5% and 5.0% TiO_2, respectively. No significant changes were observed for this parameter. However, the crystallization enthalpy (ΔH_c) of the PHBV/TiO_2 5.0% nanocomposite was more evident and exhibited a larger magnitude curve than other nanocomposites and pure PHBV, indicating that TiO_2 has a heterogeneous nucleation effect on the polymer matrix.

The second heating thermogram is shown in figure 3(c). This thermogram, after the cooling process, showed significantly different behavior when compared to that observed in the first heating. The crystallization peak in PHBV occurred in the second heating, since the cooling rate allowed a slow nucleation and, thus, the formation of crystals in the material [46]. The cold crystallization temperature (T_{cc}) appeared at low temperatures. For pure PHBV and the nanocomposites with 1.0%, 2.5% and 5.0% of TiO_2, the T_{cc} were 56.4, 55.1, 56.5 and 46.8 °C, respectively. The T_{cc} values for the PHBV/TiO_2 nanocomposites shifted slightly to lower temperature ranges when compared to the pure PHBV. This can be attributed to the parts of PHBV that crystallize during the cooling process in the presence of the TiO_2 nanoparticles, which act as nuclei for the remaining PHBV to crystallize in the second heating process. Wang *et al* [47] found the same behavior for PHBV/GNS nanocomposites.

The crystallinity degree (%C) for the second heating was calculated according to equation (3). It was noted that %C is more pronounced with high concentrations of titanium dioxide. The crystallinity degree increased from 8.5% in PHBV to 26.0% in the nanocomposite with 5.0% TiO_2, indicating that the nanoparticles acted as a nucleating agent. This occurs because the presence of nanoparticles can greatly influence the crystallization behavior of the polymeric matrix. Depending on the size and distribution, the nanoparticles can have the ability to nucleate, affecting the nucleation density, the spherulite size and the kinetics of crystallization, as well as the brittleness of the polymer [43]. Liu *et al* [48] studied the effect of adding clay to nylon 6, investigating the behavior of this system through DSC cooling curves. The authors verified that the shape and the temperature of the peaks were different for the nanocomposites when compared to the pure polymer. The presence of clay increased the crystallization temperature of nylon 6 and decreased the width of the crystallization peak. They concluded that the clay increased the crystallization rate and had a strong heterophase nucleation effect on nylon 6.

In this work, the glass transition temperature of PHBV was observed by a deflection in the second heating curve at ~0 °C. It is possible to notice that, with the incorporation of TiO_2 into the polymer, the T_g decreases. With 5.0% of nanoparticles, the T_g is −7 °C, the nanoparticles promoted the separation between the chains, weakening intermolecular interactions and resulting in an increasing in the chains general mobility in the amorphous phase.

Several authors have studied the interactions between the polymer matrix and the nanoparticles by some properties of PNC, including the glass transition temperature (T_g), which can interact attractively with the polymer to increase the T_g. Alternatively, a repulsive interaction decreases the T_g behavior related to the enthalpy of components interface due to an increase in molecular contacts on the surface of the nanoparticles [49–51].

Arantes *et al* [52] studied the effect of Laponite on the properties of PNC and observed that the presence of Laponite has opposite effects on the glass transition temperature of NBR and SBR nanocomposites. While the SBR-based materials have their T_g shifted to higher temperatures, the T_g of NBR materials slightly decreased. This apparent divergent result expresses the differences of each macromolecule. While SBR exhibits a strong interaction with the nanoparticles, which could be evaluated by the shift of T_g to higher temperatures, the weaker interaction between nanoparticles and NBR augmented the flexibility and mobility of the polymer chains, shifting the T_g to lower temperatures. Moreover, there is an increase in heat capacity variation (ΔC_p) associated with the variation of T_g related to more rigid amorphous domains in the nanocomposites, which restrict the mobility of polymer chains close to the nanoparticles.

Surface modifications of the nanoparticles with coupling agents or varying the pH can change the final properties of nanocomposites, including T_g. If a surface has attractive interactions with the polymer, T_g is increased, if the interaction is repulsive, T_g decreases and, finally, if interactions do not occur, T_g is not affected. The behavior of the system in the interfaces is defined by energetic interactions, where the interfacial properties are enthalpic effects and the entropic effects play a secondary role. The T_g modification is unfavorable by entropy and is offset by a gain in enthalpy due to increased molecular contacts promoted by the nanoparticles dispersed on the surface [53]. Thus, the studied nanocomposites may have been structured by nanoparticles with repulsive interactions with the polymer, resulting in the decrease in T_g. Zuang *et al* [4] found the opposite behavior, as they noticed an increase in the T_g of PLA/TiO_2 nanocomposites when compared to the pure polymer, because the titanium dioxide nanoparticles restricted the mobility of the PLA molecular chain. This behavior was due to hydrogen bonds formed between the carbonyl group of the PLA and the hydroxyl group at the particle surface.

DMA is defined by three parameters: the storage modulus (E'), which is the elastic response to the deformation, i.e., the material's ability to absorb energy; the loss modulus (E''), which is the response to plastic

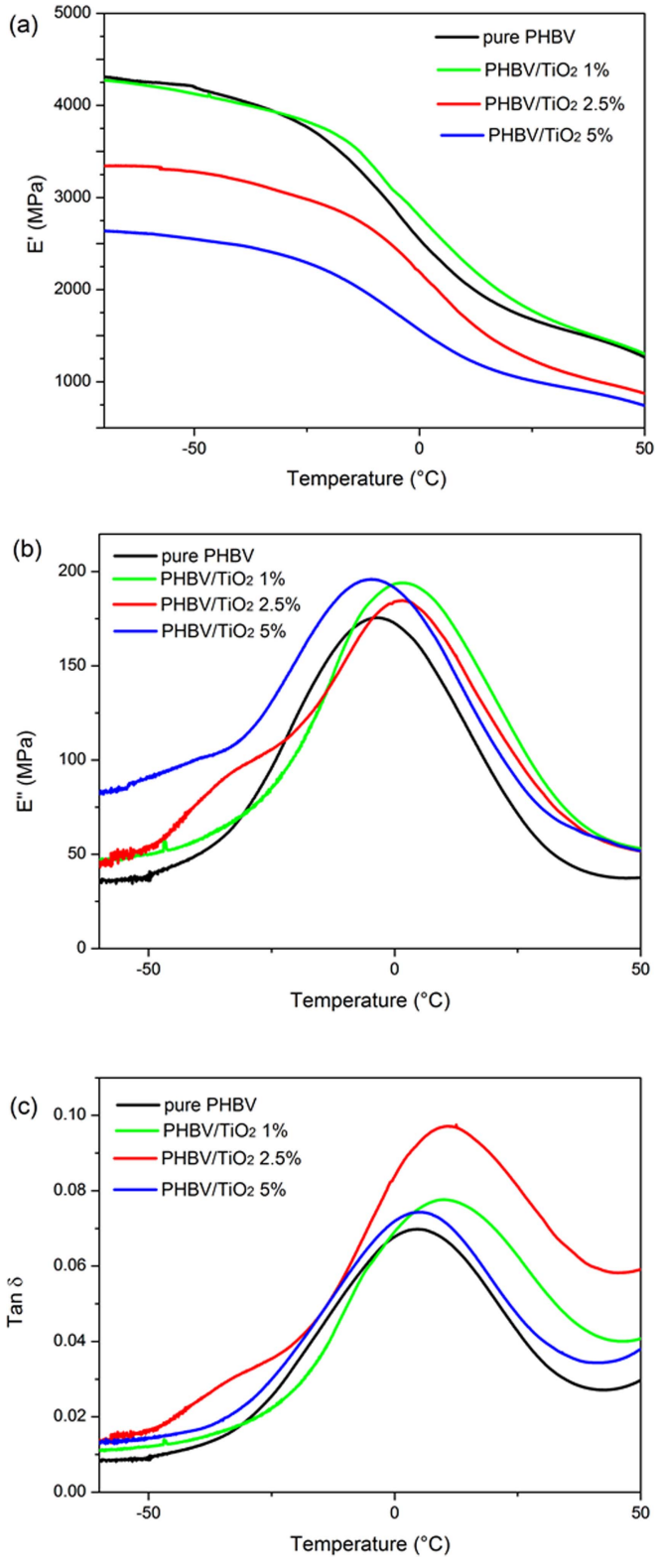

Figure 4. DMA curves of the pure PHBV and nanocomposites: (a) storage modulus (E'), (b) loss modulus (E'') and (c) tan δ.

deformation, i.e., the material ability to dissipate energy, and tan δ, which is the ratio E''/E', a measure of the damping ability of the material. The maximum peak in the tan δ curve was used to determine T_g.

Figure 4(a) shows the temperature dependence of the storage modulus (E'). It is noticed that the E' values for all samples decrease considerably with increasing temperature. This fact is due to the increased mobility of the polymer chains in higher temperatures [54]. However, for the PHBV/TiO_2 2.5% and PHBV/TiO_2 5.0% nanocomposites, E' was lower than the E' observed for pure PHBV because the high concentrations of nanoparticles in the polymer matrix can form clusters that produce breakpoints in the polymer matrix, which

Table 3. Damping properties calculated for the nanocomposites and PHBV with different titanium dioxide concentrations.

Sample	T_g (°C)	LA (MPa.K)	TA (K)	$E_{a_{AV}}$ (KJ Mol^{-1})
PHBV	4.3	9513	3.87	310.2
PHBV/TiO_2 1.0%	9.8	11 062	4.49	266.7
PHBV/TiO_2 2.5% %	10.5	11 112	5.95	227.5
PHBV/TiO_2 5.0%	5.0	12 206	4.35	149.5

reduce its mechanical strength. Moreover, agglomeration of particles at high concentrations leads to a small stress transfer in the composite [45].

Melo *et al* [54] studied the thermomechanical behavior of PHB with carnauba fiber composites with different treatments on the fiber. Through their tests, it was observed that E' was lower for the composite than for pure PHB at temperatures lower than T_g, but the value was higher at temperatures above T_g. This reduction of E' can be associated with poor fiber-matrix interfacial adhesion. Through this, it can be stated that the nanocomposites studied here also have a low storage modulus compared to pure PHBV, possibly due to poor adherence between the interface of the nanoparticles and the polymeric matrix, or due to particle agglomeration leading to a stress transfer in the matrix, thereby decreasing the mechanical strength.

Through the loss modulus (E'') analysis shown in figure 4(b), it is possible to observe two peaks in the curve for PHBV/TiO_2 2.5%, one is related to the glass transition and the other is due to a secondary transition. The secondary relaxations are relative to amorphous phases, which occur at temperatures below T_g and are classified by β, γ and δ. These molecular relaxations involve localized movement, because below T_g, the mobility of the molecular chains is reduced [55].

As observed in the tan δ curves in figure 4(c), there is a slight shift of the peak (related to T_g) to higher temperatures and there was an increase in T_g with the increase of nanoparticle concentration in the polymer matrix. This is the opposite behavior compared to the results of T_g measured by DSC, which is a less sensitive analysis. The tan δ, expressed as the ratio between E'' and E', considers the energy dissipated as heat during the dynamic test [56], also known as loss factor or damping. This parameter expresses the ability of the material to convert mechanical energy in heat [55].

The damping capacity of PHBV and the nanocomposites was evaluated from the area under the peak of the loss modulus curve (LA) and from the area under the tan δ peak (TA). The value of LA is given by:

$$\mathrm{LA} = \int_{T_1}^{T_r} E'' \mathrm{d}T = \frac{(E'_g - E'_r) R . T_g^2 (\pi/2)}{(E_a)_{AV}}, \tag{4}$$

where E'_g and E'_r are the storage modulus before and after T_g, respectively, T_g is the glass transition temperature, T_1 and T_r are the temperatures above and below T_g, respectively, $(E_a)_{AV}$ is the activation energy of the polymer relaxation process and R is the universal gas constant.

The T_g, the area under the curve of tan δ (TA), the area under the LA and the calculated values for the activation energy of PHBV for the different nanocomposites are shown in table 3.

As shown in table 3, there was an increase in the area under the curve of the LA and the tan δ versus temperature for PHBV with increasing titanium dioxide content in the nanocomposites, showing an increase in the nanocomposite damping properties when compared to the pure polymer. This increase in the area under the loss modulus curve was due to the increase in the concentration of the groups that have high capacity to dissipate mechanical energy as heat [53]. Moreover, $(E_a)_{AV}$ decreases with increasing titanium dioxide concentration, indicating that the presence of TiO_2 in the nanocomposites decreases the energy for the relaxation process, probably due to the increased hydrogen bonds present between TiO_2 and PHBV increasing the quantity of groups responsible for energy dissipation. Hourston *et al* [57] determined areas under the E'' and tan δ versus temperature curves for interpenetrating polymeric networks consisting of thermoplastic polyurethanes and poly (ethyl methacrylate) (PEMA). The area under the E'' curve gradually increased with PEMA content, reflecting the concentration of groups with higher capacity to dissipate mechanical energy. The polymer PEMA has carbonyl groups, as is the case with the polymer PHBV, indicating that this group may be responsible for mechanical energy dissipation.

3.3. Biodegradation studies

Biodegradation studies were made to simulate the action of the environment and determine the biodegradation rates. Laboratorial tests were carried out on samples of PHBV and nanocomposites. In periods of 48 h, the samples were removed from the liquid medium and washed with distilled water, and then dried in a desiccator for 1 h.

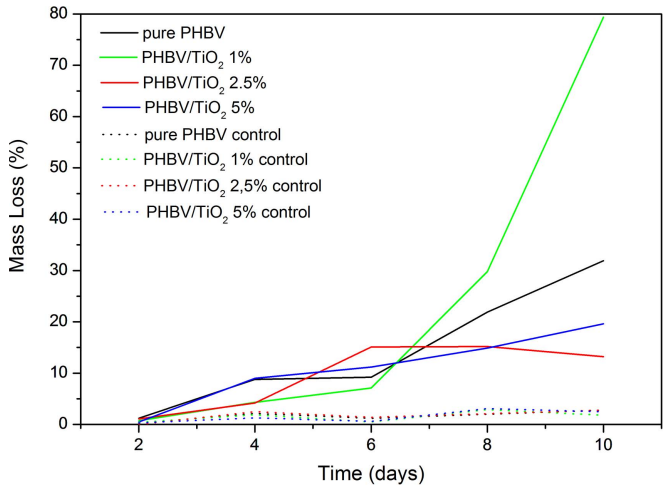

Figure 5. Results for the biodegradation of pure PHBV and nanocomposites in an aqueous medium.

The simple permanence of a sample in mineral solution could result in the loss of mass due to the physical degradation of the material. Therefore, control samples were immersed in a sterile mineral solution under the same conditions as the test (120 rpm and 30 °C). The biodegradability of the samples was determined by the weight loss over time, as can be seen in figure 5.

The results showed high activity for polymer and nanocomposite degradation for the samples immersed in the bacterial suspension, because there was a reduction of the mass of the films. The weight loss is related to factors such as the type of microorganism present, the surface areas of the samples, temperature, pH and the availability of oxygen and nutrients in the medium [58]. The maximum weight loss for PHBV reached 32% after 10 d of incubation. For the nanocomposite with 1.0% TiO_2, the weight loss after 10 d was higher, reaching 79% due to the fragility of the specimen that fell apart when washed. This result indicates the high biodegradability of this nanocomposite during the studied period, possibly related to greater homogeneity that this nanocomposite with 1.0% TiO_2 has in relation to other nanocomposites. It can be observed that the weight loss of all control samples remained constant over time, indicating that degradation due to physical factors, such as temperature and stirring, do not interfere significantly in the result for the biodegradation of the materials [59].

For the biodegradation study in soil, samples were buried for a period of up to 20 d. Every 5 d the material was analyzed to determine the weight loss and photographed to verify the occurrence of macroscopic changes in the samples with the time of contact with the soil. Figure 6 shows the macroscopic changes in the samples that were buried and retrieved every 5 d of incubation compared to the control samples (not buried).

The biodegradability of the samples was determined by the weight loss over time, as can be seen in the graph presented in figure 7. In table 4, the average weight loss values obtained from figure 7 are summarized. These results provide clear evidence that, as the time of contact with the soil increased for the samples, the weight loss increased, but not in a proportional manner.

When removed from the soil, all samples presented a considerable mass of soil adhered on their surfaces. After washing, the loss of some physical properties of the PHBV and nanocomposites was observed, such as loss of the gloss on the surface. Some changes were also observed, such as the appearance of pitting and cracks. In the case of the nanocomposites, the weight loss was more evident because of the presence of oxidizing groups formed on the surface of the titanium dioxide, breaking the polymer chain [35]. The surface of the samples showed higher degradation, weakness and loss of dimensions, including the formation of holes. The films clearly showed morphological and structural changes after 20 d buried in the soil, characterizing the biodegradation process. The changes were attributed to the enzymatic action of microorganisms present in the soil, which caused oxidative reactions and/or rearrangements in the polymer chain [60]. During the test, the PHBV films were either digested by the microorganisms or broken into small fragments.

Several studies of the biodegradation rate for the PHBV polymer in soil can be found in the literature. Kuntanoo *et al* [61] observed that the percentage of degradation of PHBV films in soil was 20% after 45 d. Gonçalves *et al* [60] buried pure PHBV in soil and noticed that, after 30 d, it was completely degraded. Yew *et al* [62] studied the biodegradation in soil of polyhydroxybutyrate films containing titanium dioxide. In their study, the films were buried in the soil and the results indicated that, in comparison to the pure PHB films, the composite films displayed slower degradation rates, indicating that the presence of the TiO_2 photocatalyst actually slows down the progress of degradation by the microorganisms present in the soil.

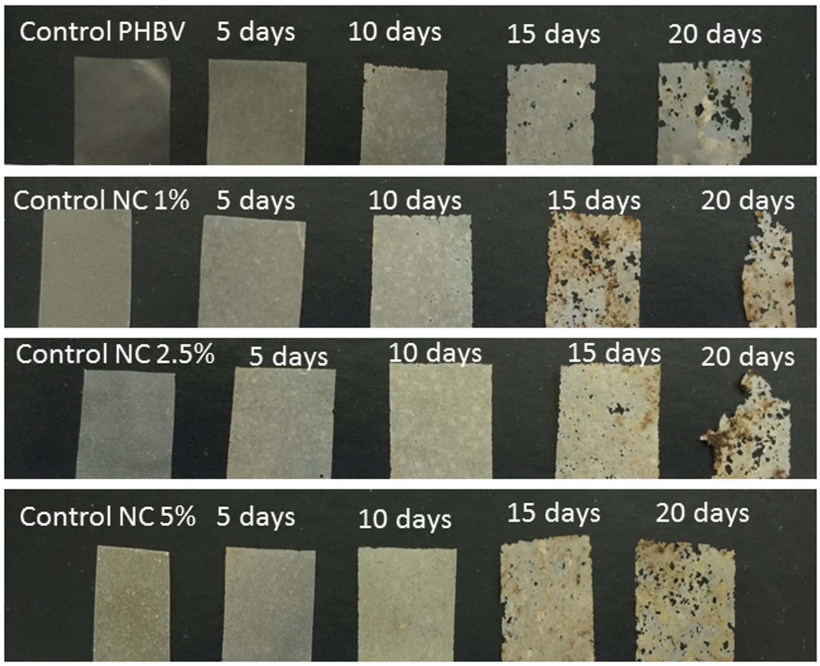

Figure 6. PHBV and nanocomposite samples submitted to biodegradation in soil.

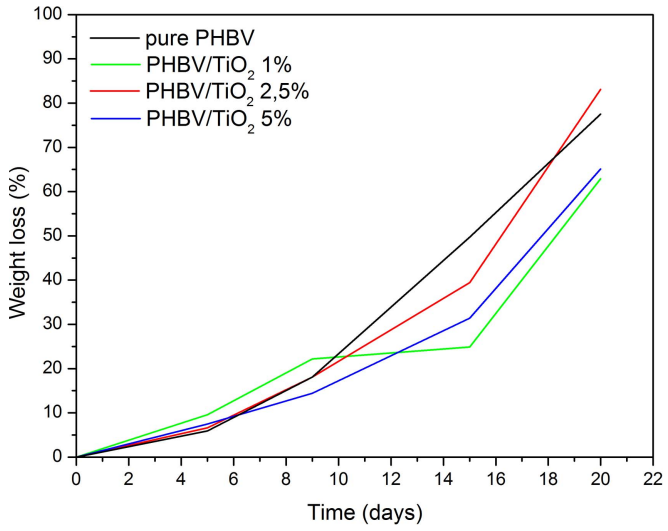

Figure 7. Results for the biodegradation of the pure PHBV and nanocomposites in soil.

Table 4. Tests results for the biodegradation of PHBV and the nanocomposites in soil.

	Weight loss (%)			
Sample	5 d	10 d	15 d	20 d
PHBV	5.9	18.1	49.7	77.5
PHBV/TiO_2 1.0%	9.6	22.2	24.9	72.9
PHBV/TiO_2 2.5%	6.6	18.1	39.4	62.9
PHBV/TiO_2 5.0%	7.5	14.4	31.4	83.1

4. Conclusions

Titanium dioxide nanoparticles were successfully obtained, exhibiting a mixture of anatase and rutile phases, by the hydrothermal method. The rutile phase had a nanorod morphology with dimensions of 40 nm in length and 12 nm in width. These nanoparticles were added to a polymer PHBV matrix by the solvent casting technique with different concentrations of 1.0%, 2.5% and 5.0% and were characterized by DSC. It was observed that the inclusion of TiO_2 in the polymer matrix decreases the glass transition temperature of the material. Alternatively, DMA analysis showed the opposite behavior. The materials were submitted to biodegradation tests. Analyzing the loss of mass, it was concluded that all samples were degraded by biotic processes, in tests with both aqueous medium and garden soil. The PHBV remained biodegradable even after the insertion of TiO_2 nanoparticles in the polymer matrix. On this basis, we can conclude that the biodegradability of PHBV was not impaired by the presence of nanoparticles. Thus, enabling the use of such nanocomposites in applications requiring biodegradable materials.

Acknowledgments

The authors gratefully acknowledge the financial supported from the Brazilian research funding agencies CNPq and FAPESP (grant no. 2013/14954-6).

ORCID iDs

Natália F Braga https://orcid.org/0000-0001-5735-7148

References

[1] Siracusa V, Rocculi P, Romani S and Rosa M D 2008 Biodegradable polymers for food packaging: a review *Trends Food Sci. Technol.* **19** 634–43
[2] Sultana N and Wang M 2012 Fabrication of tissue engineering scaffolds using the emulsion freezing/freeze-drying technique and characteristics of the scaffolds *Integrated Biomaterials in Tissue Engineering* ed M Ramalingham, Z Haider, S Ramakrishna, H Kobayashi and Y Haikel (Hoboken, NJ: Wiley) ch 4 pp 63–89
[3] Li W, Nooeaid P, Roether J A, Schubert D W and Boccaccini A R 2014 Preparation and characterization of vancomycin releasing PHBV coated 45S5 bioglass ® -based glass—ceramic scaffolds for bone tissue engineering *J. Eur. Ceram. Soc.* **34** 505–14
[4] Zhuang W, Liu J, Zhang J H, Hu B X and Shen J 2009 Preparation, characterization, and properties of TiO_2/PLA nanocomposites by *in situ* polymerization *Polym. Compos.* **30** 1074–80
[5] Armentano I, Dottori M, Fortunati E, Mattioli S and Kenny J M 2010 Biodegradable polymer matrix nanocomposites for tissue engineering : a review *Polym. Degrad. Stab.* **95** 2126–46
[6] Camargo P H C, Satyanarayana K G and Wypych F 2009 Nanocomposites: synthesis, structure, properties and new application opportunities *Mater. Res.* **12** 1–39
[7] Ten E, Turtle J, Bahr D, Jiang L and Wolcott M 2010 Thermal and mechanical properties of poly(3-hydroxybutyrate-co-3-hydroxyvalerate)/cellulose nanowhiskers composites *Polymer* **51** 2652–60
[8] Rajh T, Dimitrijevic N M, Bissonnette M, Koritarov T and Konda V 2014 Titanium dioxide in the service of the biomedical revolution *Chem. Rev.* **114** 10177–216
[9] Mofokeng J P and Luyt A S 2015 Morphology and thermal degradation studies of melt-mixed poly(hydroxybutyrate-co-valerate) (PHBV)/poly(e-caprolactone) (PCL) biodegradable polymer blend nanocomposites with TiO_2 as filler *J. Mater. Sci.* **50** 3812–24
[10] Mofokeng J P and Luyt A S 2015 Morphology and thermal degradation studies of melt-mixed PLA/PHBV biodegradable polymer blend nanocomposites with TiO_2 as filler *J. Appl. Polym. Sci.* **132** 42138
[11] Dinari M and Asadi P 2015 Thermal, mechanical and optical transport properties of nanocomposite materials based on triethoxysilane-terminated polyimide and TiO_2 nanoparticles *RSC Adv.* **5** 60745–53
[12] Mallakpour S and Dinari M 2012 Fabrication of polyimide/titania nanocomposites containing benzimidazole side groups via sol–gel process *Prog. Org. Coat.* **75** 373–8
[13] Dinari M and Ahmadizadegan H 2014 Synthesis, structural characterization and properties of novel functional poly(ether imide)/titania nanocomposite thin films *Polymer* **55** 6252–60
[14] Mofokeng J P and Luyt A S 2015 Dynamic mechanical properties of PLA/PHBV, PLA/PCL, PHBV/PCL blends and their nanocomposites with TiO_2 as nanofiller *Thermochim. Acta.* **613** 41–53
[15] Kim J-H, Sheikh F, Ju H W, Park H J, Moon B M, Lee O J and Park C H 2014 3D silk fibroin scaffold incorporating titanium dioxide (TiO_2) nanoparticle (NPs) for tissue engineering *Int. J. Biol. Macromol.* **68** 158–68
[16] Kar A, Raja K S and Misra M 2006 Electrodeposition of hydroxyapatite onto nanotubular TiO_2 for implant applications *Surf. Coat. Technol.* **201** 3723–31
[17] Santos A R, Barbanti S H, Duek E A R, Dolder H, Wada R S and Wada M L F 2001 Vero cell growth and differentiation on poly(L-lactic acid) membranes of different pore diameters *Artif. Organs* **25** 7–13
[18] Dewez J L, Lhoest J B, Detrait E, Berger V, Dupont-Gillain C C, Vincent L M, Schneider Y J, Bertrand P and Rouxhet P G 1998 Adhesion of mammalian cells to polymer surfaces: from physical chemistry of surfaces to selective adhesion on defined patterns *Biomaterials* **19** 1441–5
[19] Santos A R Jr and Wada M L F 2007 Polímeros biorreabsorvíveis como substrato para cultura de células e engenharia tecidual *Polímeros Ciência E Tecnol.* **17** 308–17

[20] Lin C-M and Yen S-K 2006 Biomimetic growth of apatite on electrolytic TiO_2 coatings in simulated body fluid *Mater. Sci. Eng.* C **26** 54–64

[21] Lee J-H, Kim S-E, Kim Y-J, Chi C-S and Oh H-J 2006 Effects of microstructure of anodic titania on the formation of bioactive compounds *Mater. Chem. Phys.* **98** 39–43

[22] Ribeiro C, Vila C, Stroppa D B, Mastelaro V R, Bettini J, Longo E and Leite E R 2007 Anisotropic growth of oxide nanocrystals: insights into the rutile TiO_2 phase *J. Phys. Chem.* C **111** 5871–5

[23] Arantes T M 2009 Incorporação por via coloidal de nanopartículas sintéticas em polímeros comerciais *Master's Thesis* Cent. Ciências Exatas E Tecnol. Dep. Química, Univ. Fed. São Carlos http://www.dominiopublico.gov.br/pesquisa/DetalheObraForm.do?select_action=&co_obra=147276

[24] Hong L W and Yu J 2003 Environmental factors and kinetics of microbial degradation of poly (3-hydroxybutyrate-co-3-hydroxyvalerate) in an aqueous medium *J. Appl. Polym. Sci.* **87** 205–13

[25] Silva A P, Montanheiro T L A, Montagna L S and Lemes A P 2017 Characterization of films of PHBV/cellulose nanocrystals nanocomposites after biodegradation in liquid medium *7th NANOMAT—Lat. Am. Conf. Metastable Nanostructured Mater. 2017 (Brotas, Brasil)* http://nanomat.dema.ufscar.br/abstracts/Abstracts/poster2/P2_08_Ana%20Paula%20da%20Silva_1.pdf

[26] Silva A P, Duran N and Lemes A P 2013 Study of biodegradation of PHBV/carbon nanotubes nanocomposites *17th Int. Conf. Compos. Struct. 2013 (Porto, Portugal)*

[27] Ayllón J A, Figueras A, Garelik S, Spirkova L, Durand J and Cot L 1999 Preparation of TiO_2 powder using titanium tetraisopropoxide decomposition in a plasma enhanced chemical vapor deposition (PECVD) reactor *J. Mater. Sci. Lett.* **18** 1319–21

[28] Akhtar M K, Xiong Y and Pratsinis S E 1991 Vapor synthesis of titania powder by titanium tetrachloride oxidation *AIche J.* **37** 1561–70

[29] Pratsinis S E 1998 Flame aerosol synthesis of ceramic powders *Prog. Energy Combust. Sci.* **24** 197–219

[30] Stoller M, Mescia M, Peroni V C and Chianese A 2007 Production of nanoparticles of titanium dioxide by using a spinning disc reactor *Chem. Eng. Trans.* **11** 71–4 http://www.aidic.it/cet/07/11/012.pdf

[31] Cargnello M, Gordon T R and Murray C B 2014 Solution-phase synthesis of titanium dioxide nanoparticles and nanocrystals *Chem. Rev.* **114** 9319–45

[32] Keswani R K, Ghodke H, Sarkar D, Khilar K C and Srinivasa R S 2010 Room temperature synthesis of titanium dioxide nanoparticles of different phases in water in oil microemulsion *Colloids Surf.* A **369** 75–81

[33] Devi R S, Venckatesh D R and Sivaraj D R 2014 Synthesis of titanium dioxide nanoparticles by sol–gel technique *Int. J. Innov. Res. Sci. Eng. Technol.* **3** 15206–11

[34] Anwar N S, Kassim A, Lim H N, Zakarya S A and Huang N M 2010 Synthesis of titanium dioxide nanoparticles via sucrose ester micelle-mediated hydrothermal processing route *Sains Malaysiana* **39** 261–5 http://www.ukm.my/jsm/pdf_files/SM-PDF-39-2-2010/15%20Anwar.pdf

[35] Arantes T M, Leite E R, Longo E and Camargo E R 2009 Nanocomposites of styrene—butadiene rubber and synthetic anatase obtained by a colloidal route and their photooxidation *J. Appl. Polym. Sci.* **113** 1898–904

[36] Yndira R, Padilla C, Matos J, Tinoco A, Lima A S, Silva D P, Mara C and Soares F 2011 Propriedades morfológicas e físico-químicas da lipase Candida rugosa imobilizada em poli (3-hidroxibutirato-co- hidroxivalerato) *18th Simpósio Nac. Bioprocessos* pp 1–6 http://openrit.grupotiradentes.com/xmlui/bitstream/handle/set/397/Cabrera-Padilla_S2_.pdf?sequence=1

[37] Liu Q-S, Zhu M-F, Wu W-H and Qin Z-Y 2009 Reducing the formation of six-membered ring ester during thermal degradation of biodegradable PHBV to enhance its thermal stability *Polym. Degrad. Stab.* **94** 18–24

[38] Nakayama N and Hayashi T 2007 Preparation and characterization of poly(l-lactic acid)/TiO_2 nanoparticle nanocomposite films with high transparency and efficient photodegradability *Polym. Degrad. Stab.* **92** 1255–64

[39] Peng X, Ding E and Xue F 2012 *In situ* synthesis of TiO_2/polyethylene terephthalate hybrid nanocomposites at low temperature *Appl. Surf. Sci.* **258** 6564–70

[40] Thiré R M D S M, Arruda L C and Barreto L S 2011 Morphology and thermal properties of poly(3-hydroxybutyrate-co-3-hydroxyvalerate)/attapulgite nanocomposites *Mater. Res.* **14** 340–4

[41] Gunaratne L M W K and Shanks R 2005 Multiple melting behaviour of poly(3-hydroxybutyrate-co-hydroxyvalerate) using step-scan DSC *Eur. Polym. J.* **41** 2980–8

[42] Casarin S A 2010 Blendas de PHBV e PCL para uso em dispositivos de osteossíntese *PhD Thesis* Cent. Ciências Exatas E Tecnol. Univ. Fed. São Carlos https://repositorio.ufscar.br/handle/ufscar/678

[43] Buzarovska A, Grozdanov A, Avella M, Gentile G and Errico M 2009 Poly (hydroxybutyrate-co-hydroxyvalerate)/titanium dioxide nanocomposites: a degradation study *J. Appl. Polym. Sci.* **114** 3118–24

[44] Dagnon K L, Chen H H, Innocentini-Mei L H and Souza N A 2009 Poly[(3-hydroxybutyrate)-co-(3-hydroxyvalerate)]/layered double hydroxide nanocomposites *Polym. Int.* **58** 133–41

[45] Vidhate S, Innocentini-mei L and Souza N A D 2012 Mechanical and electrical multifunctional poly (3-hydroxybutyrate-co-3-hydroxyvalerate)—multiwall carbon nanotube nanocomposites *Polym. Eng. Sci.* **52** 1367–74

[46] Ferreira B M P, Zavaglia C A C and Duek E A R 2002 Films of PLLA/PHBV: thermal, morphological, and mechanical characterization *J. Appl. Polym. Sci.* **86** 2898–906

[47] Wang B, Zhang Y, Zhang J, Gou Q, Wang Z, Chen P and Gu Q 2013 Crystallization behavior, thermal and mechanical properties of PHBV/graphene nanosheet composites *Chin. J. Polym. Sci.* **31** 670–8

[48] Liu L, Qi Z and Zhu X 1999 Studies on nylon 6/clay nanocomposites by melt-intercalation process *J. Appl. Polym. Sci.* **71** 1133–8

[49] Schadler L S, Kumar S K, Benicewicz B C, Lewis S L and Harton S E 2007 Designed interfaces in polymer nanocomposites: a fundamental viewpoint *MRS Bull.* **32** 335–40

[50] Mackay M E, Tuteja A, Duxbury P M, Hawker C J, Horn B V, Guan Z, Chen G and Krishnan R S 2006 General strategies for nanoparticle dispersion *Science* **311** 1740–3

[51] Barick A K and Tripathy D K 2010 Thermal and dynamic mechanical characterization of thermoplastic polyurethane/organoclay nanocomposites prepared by melt compounding *Mater. Sci. Eng.* A **527** 812–23

[52] Arantes T M, Sala R L, Longo E, Leite E R, Paranhos C M and Camargo E R 2017 Elastomeric clay nanocomposites prepared by colloidal route: study of interrelationship of structure and physical-chemistry properties *J. Nanosci. Nanotechnol. Appl.* **1** 101–14 http://article.scholarena.co/Elastomeric-Clay-Nanocomposites-Prepared-by-Colloidal-Route-Study-of-Interrelationship-of-Structure-and-Physical-Chemistry-Properties.pdf

[53] Arantes T M 2012 Modificação das Propriedades dos Polímeros Comerciais de SBR e NBR a Partir da Incorporação de Nanopartículas Sintéticas *PhD Thesis* Cent. Ciências Exatas E Tecnol. Dep. Química, Univ. Fed. São Carlos LINK: https://repositorio.ufscar.br/handle/ufscar/6226

[54] Melo J D D, Carvalho L F M, Medeiros A M, Souto C R O and Paskocimas C A 2012 A biodegradable composite material based on polyhydroxybutyrate (PHB) and carnauba fibers *Composites* B **43** 2827–35
[55] Cassu S N and Felisberti M I 2005 Comportamento dinâmico-mecânico e relaxações em polímeros e blendas poliméricas *Quim. Nov.* **28** 255–63
[56] Singh S, Mohanty A K, Sugie T, Takai Y and Hamada H 2008 Renewable resource based biocomposites from natural fiber and polyhydroxybutyrate-co-valerate (PHBV) bioplastic *Composites* A **39** 875–86
[57] Hourston D J and Schafer F-U 1996 Damping characteristics of polyurethane-based simultaneous interpenetrating polymer networks *High Perform. Polym.* **8** 19–34
[58] Bucci D Z, Tavares L B B and Sell I 2007 Biodegradation and physical evaluation of PHB packaging *Polym. Test.* **26** 908–15
[59] Lemes A P 2005 Desenvolvimento de novos compósitos biodegradáveis baseados em poli(3-hidroxibutirato- co- hidroxivalerato) e lignosulfonatos *Master's Thesis* Univ. Federal de Campinas, Instituto de Química http://repositorio.unicamp.br/handle/REPOSIP/248905
[60] Gonçalves S P C, Martins-Franchetti S M and Chinaglia D L 2009 Biodegradation of the films of PP, PHBV and its blend in soil *J. Polym. Environ.* **17** 280–5
[61] Kuntanoo K, Promkotra S and Kaewkannetra P 2013 Biodegradation of polyhydroxybutyrate-co- hydroxyvalerate (PHBV) blended with natural rubber in soil environment *World Acad. Sci. Eng. Technol.* **7** 1057–61 http://waset.org/publications/16662/biodegradation-of-polyhydroxybutyrate-co-hydroxyvalerate-phbv-blended-with-natural-rubber-in-soil-environment
[62] Yew S P, Tang H Y and Sudesh K 2006 Photocatalytic activity and biodegradation of polyhydroxybutyrate films containing titanium dioxide *Polym. Degrad. Stab.* **91** 1800–7